

Critical Casimir interactions and colloidal self-assembly in near-critical solvents

Nikos Tasios, John R. Edison, René van Roij, Robert Evans, and Marjolein Dijkstra

Citation: *The Journal of Chemical Physics* **145**, 084902 (2016); doi: 10.1063/1.4961437

View online: <http://dx.doi.org/10.1063/1.4961437>

View Table of Contents: <http://scitation.aip.org/content/aip/journal/jcp/145/8?ver=pdfcov>

Published by the **AIP Publishing**

Articles you may be interested in

[Effective interaction between a colloid and a soft interface near criticality](#)

J. Chem. Phys. **141**, 134704 (2014); 10.1063/1.4896383

[Tuning effective interactions close to the critical point in colloidal suspensions](#)

J. Chem. Phys. **137**, 084903 (2012); 10.1063/1.4745479

[Phase behavior of colloidal suspensions with critical solvents in terms of effective interactions](#)

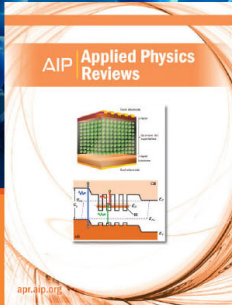
J. Chem. Phys. **136**, 224902 (2012); 10.1063/1.4722883

[Critical Casimir effect for colloids close to chemically patterned substrates](#)

J. Chem. Phys. **133**, 074702 (2010); 10.1063/1.3464770

[Cosurfactant and cosolvent effects on surfactant self-assembly in supercritical carbon dioxide](#)

J. Chem. Phys. **122**, 094710 (2005); 10.1063/1.1855291



NEW Special Topic Sections

NOW ONLINE
Lithium Niobate Properties and Applications:
Reviews of Emerging Trends

AIP | Applied Physics
Reviews

Critical Casimir interactions and colloidal self-assembly in near-critical solvents

Nikos Tasios,¹ John R. Edison,² René van Roij,³ Robert Evans,⁴ and Marjolein Dijkstra^{1,a)}

¹*Soft Condensed Matter, Debye Institute for Nanomaterials Science, Utrecht University, Princetonplein 1, 3584 CC Utrecht, The Netherlands*

²*Molecular Foundry, Lawrence Berkeley National Laboratory, 1 Cyclotron Road, Berkeley, California 94720, USA*

³*Institute for Theoretical Physics, Utrecht University, Princetonplein 5, 3584 CC Utrecht, The Netherlands*

⁴*H. H. Wills Physics Laboratory, University of Bristol, Bristol BS8 1TL, United Kingdom*

(Received 23 June 2016; accepted 9 August 2016; published online 22 August 2016)

A binary solvent mixture close to critical demixing experiences fluctuations whose correlation length, ξ , diverges as the critical point is approached. The solvent-mediated (SM) interaction that arises between a pair of colloids immersed in such a near-critical solvent can be long-ranged and this so-called critical Casimir interaction is well-studied. How a (dense) suspension of colloids will self-assemble under these conditions is poorly understood. Using a two-dimensional lattice model for the solvent and hard disks to represent the colloids, we perform extensive Monte Carlo simulations to investigate the phase behaviour of this model colloidal suspension as a function of colloid size and wettability under conditions where the solvent reservoir is supercritical. Unlike most other approaches, where the solvent is modelled as an implicit background, our model employs an explicit solvent and treats the suspension as a ternary mixture. This enables us to capture important features, including the pronounced fractionation of the solvent in the coexisting colloidal phases, of this complex system. We also present results for the partial structure factors; these shed light on the critical behaviour in the ternary mixture. The degree to which an effective two-body pair potential description can describe the phase behaviour and structure of the colloidal suspension is discussed briefly. *Published by AIP Publishing.* [<http://dx.doi.org/10.1063/1.4961437>]

I. INTRODUCTION

Colloidal particles suspended in a solvent can display a rich variety of effective interactions. Well-known examples include depletion, arising from the presence of additional, smaller components (depletants), and the Derjaguin-Landau-Verwey-Overbeek (DLVO) interaction arising from screening by counterions in the case of a charge-stabilised colloidal suspension. Theoretical treatments of effective interactions between colloids usually proceed by tracing out the degrees of freedom of the smaller components, i.e., depletants and ions, assuming that the underlying molecular solvent is merely an “inert” structureless background. However, there are several situations where the thermodynamic state of the solvent plays a key role leading to characteristic solvent-mediated (SM) interactions between colloids. In particular, for certain colloidal suspensions, long-ranged SM interactions can arise due to the local fluctuations of the solvent composition. An important situation occurs when the solvent is close to its (demixing) critical point. Then the SM interaction between two colloidal particles becomes long-ranged; the range is set by the (diverging) correlation length, ξ , of the solvent mixture. This is the situation we consider in the present paper where we investigate the properties of a model of a ternary mixture that mimics colloidal particles suspended in an explicit binary solvent near its critical point. The model and some preliminary

results for the colloidal phase behaviour were introduced in Ref. 1. Here we describe the Monte Carlo (MC) simulation methods and present a comprehensive set of results for the phase behaviour and structural properties of the same (lattice) model.

We motivate our study by recalling first the properties of a binary AB solvent mixture near its demixing critical point. Figure 1 shows a schematic phase diagram of such a mixture in the reduced temperature, $\tau = (T - T_c)/T_c$, versus composition, $x_r = N_B/(N_A + N_B)$, representation, with T the temperature, T_c the critical temperature, and $N_{A(B)}$ the number of particles of solvent $A(B)$. The solvent has an upper critical solution temperature, denoted by the red circle. The critical point occurs at $\tau = 0$ and at critical composition, $x_{r,c} = 1/2$. For $\tau < 0$ the phase diagram exhibits a two-phase region, where the solvent mixture demixes into an A -rich and a B -rich phase. The binodal in Fig. 1 is symmetric about $x_r = 1/2$ as the solvent model employed here has Ising or lattice gas symmetry. The approach to criticality is signalled by the presence of fluctuations in the order parameter, in this case composition, occurring on increasing length scales, up to the bulk correlation length of the solvent, ξ . Sufficiently close to the critical point, $\xi \sim |\tau|^{-\nu}$, where ν is a critical exponent characteristic of the particular universality class of the system.

Suppose now the solvent comes into contact with a substrate (plate), or a large colloidal particle, that prefers one of the solvent species, say B . The local composition of the solvent close to the surface will be enriched with that species.

^{a)}Electronic mail: m.dijkstra@uu.nl

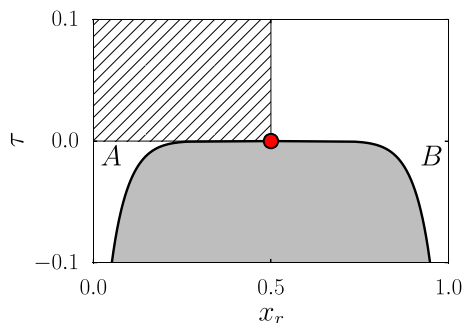


FIG. 1. Phase diagram of a binary AB solvent mixture in the reduced temperature, $\tau = (T - T_c)/T_c$, versus composition, x_r , representation. The grey area denotes the two-phase region, where the solvent mixture demixes in an A -rich and a B -rich phase. The phases coexist on the binodal (solid line) and the critical point is indicated by the red circle. The hatched box indicates the (supercritical, A -rich) region investigated in this study.

If the solvent is close to its critical point, the red circle in Fig. 1, the length scale over which the composition profile approaches the bulk composition is set by the correlation length, ξ . This is the well-known phenomenon of critical adsorption, see e.g., Ref. 2. When the near-critical fluid is confined between two plates, or two large colloids, one expects that the critical adsorption at each surface will lead to interesting SM interactions. Indeed Fisher and de Gennes showed in 1978³ that when two plates, at a separation $L \sim \xi$, are immersed in such a solvent mixture these will experience a long-ranged SM interaction. Exactly at the critical point, the SM force between plates decays algebraically, i.e., as L^{-D} , where D is the bulk spatial dimension. The interaction is attractive if the two plates are identical or preferentially adsorb the same solvent species, but can be repulsive if they adsorb opposite species. In recent times this effect has been termed the *critical Casimir effect*,⁴⁻⁶ due to the similarities it shares with the celebrated Casimir effect. In the latter, an algebraically decaying force is induced between two conducting macroscopic bodies as a consequence of confining quantum fluctuations of the electromagnetic field.⁷ Theoretical and simulation studies of critical Casimir interactions in planar wall confinement are numerous; see, for example, Refs. 4-6, 8, and 9. The scaling behaviour of the SM force, i.e., how it depends on L/ξ , has been determined for various universality classes and various choices of boundary conditions. Results for two parallel plates can be extended to a sphere near a plate and to a pair of large spherical colloids using the Derjaguin approximation.¹⁰ Accepting concepts of universality, and that real fluid mixtures lie in the 3D Ising universality class, we can argue that from theory and simulation we now have a rather good description of the effective pair interaction, at large inter-particle separations, between an isolated pair of identical colloidal particles suspended in a solvent at its critical composition $x_{r,c}$. For off-critical compositions the scaling behaviour of the critical Casimir interaction is more complicated but there has been recent progress in ascertaining this; see Refs. 11-13 and references therein. Moreover, the results of direct experimental measurements of the critical Casimir force between a colloid and a planar substrate, using total internal reflection microscopy,^{14,15} confirm the form of the

predicted scaling functions. A forthcoming review¹⁶ provides a comprehensive account of this subject.

Suppose now we move up in complexity and enquire what is the phase behaviour and structure of a dense suspension of identical colloids in the same near-critical solvent. The critical Casimir effect might well be expected to play an important role in colloidal aggregation and phase behaviour; long-ranged SM interactions should be present close to the critical point of the solvent. The history is interesting. Probably the first experimental observation of colloidal aggregation in a near-critical solvent goes back to the work of Beysens and Estève¹⁷ in 1985. In this experiment, silica spheres, with diameter 160 nm, preferentially adsorbing lutidine, were suspended in a water-lutidine mixture. Beysens and Estève measured the temperature at which the silica particles began to form aggregates upon heating the ternary mixture, which allowed them to determine an “aggregation line” in the composition-temperature diagram. This aggregation line resided on the water-rich side of the phase diagram and the authors first associated this with the prewetting line that might be linked with preferential adsorption of lutidine at a single macroscopic substrate. However, the line extended to temperatures in the one-phase region below the demixing critical point, which is not found for prewetting lines at a planar substrate. Note that the water-lutidine mixture exhibits a demixing phase transition above a lower critical temperature rather than demixing below an upper critical temperature, as shown in Figure 1. Transcribing to our present model, the observed aggregation line extended to the region $\tau > 0$, on the A -rich side of the phase diagram supposing species B to be preferentially adsorbed on the colloids, indicated by the hatched region in Figure 1. Several other experimental studies followed, using different solvents and colloids.¹⁸⁻²⁴ In addition the effect of adding salt was investigated²⁵ and it was found that adding sufficient Mg^{2+} ions resulted in the aggregation line flipping from the lutidine-rich phase to the water-rich phase. The phenomenon of reversible colloidal aggregation in near-critical solvents appears to be quite general. A brief review²⁶ summarizes the state of play up to 1999. Although the precise location of the aggregation line depends on a complex interplay of van der Waals (dispersion), screened Coulomb, and adsorption-induced long-ranged effective interactions, reversible aggregation appears to occur generally in near-critical binary solvents at compositions, near the binodal, that are poor in the species preferentially adsorbed by the colloidal particle. Note that this is the region of the solvent phase diagram where the critical Casimir attraction between two identical colloids is expected to be strongest.^{11,27,28}

Pertinent to our present study is the experimental work of Kaler *et al.*^{21,22} who argued that the system of colloids in a binary solvent mixture should be viewed as a true ternary mixture including full fractionation of the components of the solvent. On the theoretical side, Sluckin²⁹ had argued already in 1990 that colloidal aggregation should be regarded as phase separation in a ternary system. Löwen,³⁰ Netz³¹ and Gil *et al.*³² followed this line, but focused on the subcritical, $\tau < 0$, region of the pure solvent reservoir, where capillary bridging between colloids brought about by wetting is likely to be the dominant mechanism in driving the colloidal aggregation. The view that

reversible aggregation is a manifestation of colloidal phase transitions was reinforced strongly by experimental studies in 2008 by Guo *et al.*³³ who carried out small-angle X-ray scattering (SAXS) studies on density-matched polystyrene particles in a solvent of water, heavy-water and picoline. The measured structure factors revealed colloidal gas, liquid, and fcc crystalline phases as the temperature was increased towards the solvent binodal at an off-critical composition. Maciolek and Dietrich¹⁶ provide a valuable overview of early experimental and theoretical work.

The same article reviews recent studies, e.g., Refs. 11–13, which construct an effective pair potential between the colloids, incorporating the long-ranged critical Casimir attraction and some empirically determined short-ranged repulsion, that is then used to investigate the properties of a dense near-critical suspension. Specifically, by extracting the attractive part of the effective pair potential from MC simulations and using liquid state theories, Mohry *et al.* investigated the phase behaviour, structure, and aggregation of an effective one-component model of a colloid-solvent mixture near the solvent's critical point. The papers of Nguyen *et al.* and Dang *et al.* adopt a similar philosophy to Mohry *et al.* but use instead an effective pair potential extracted from experimental measurements of the colloid-colloid pair correlation function.^{34,35} The results are summarized in another topical review,³⁶ more experimentally focussed, which outlines important and exciting possibilities for reversible colloidal particle assembly brought about by tuning the temperature and composition of an appropriate host solvent. The title of this review “Critical Casimir Forces for Colloidal Assembly” is revealing. Indeed the authors argue strongly that an effective pair potential description, which incorporates critical Casimir attraction, should be sufficient to capture most of the physics relevant for colloidal phase behaviour.

The extent to which a one-component description, incorporating only pairwise effective interactions between the colloids, might be accurate for a dense suspension is not at all obvious. Very close to solvent criticality, where the solvent correlation length ξ can be several times the colloid radius, the inter-particle forces are long-ranged, and one must expect that many-body effects are important. Consequently, in this regime, an effective pair potential description should break down — perhaps not in the qualitative description of colloidal phase behaviour but certainly in a quantitative description. At off-critical compositions, further from criticality, where ξ is considerably smaller than the colloid radius, one might hope that the effective pair potential description is better founded and this is the viewpoint taken in both recent reviews.^{16,36}

In order to address such issues it is necessary to investigate in detail the phase behaviour of a ternary colloid-AB solvent mixture. We employ the same 2D lattice model of such a system as used in our preliminary study¹ where we focused on the supercritical region of the solvent phase diagram and found rich colloidal phase behaviour, including a broad gas-solid coexistence and a pronounced shift of the critical point of the ternary mixture with respect to that of the pure AB solvent. Our present study is also motivated partly by work of Edison *et al.* who developed a mean-field theory, based on free-volume arguments,³⁷ that describes the phase

behaviour of the same model; we shall allude to this later. Here we describe an extensive MC simulation study of the phase behaviour and partial structure factors of the lattice model that extends substantially the results presented in Ref. 1. Specifically, we provide results for the effects of colloid size and wettability (strength of the preferential adsorption) on the phase behaviour of the ternary mixture and, in addition, we present some new results for the effective pair interactions between colloids under different conditions of the solvent reservoir, that is in diffusive (osmotic) equilibrium with the suspension. Moreover, details on the computational methods are provided; these were not given in Ref. 1. We continue to focus on the supercritical, $\tau > 0$, region of the pure solvent mixture phase diagram, where wetting-induced interactions such as capillary bridging are absent. The latter can be very strong and could potentially mask the subtle effects of the critical Casimir interactions. Our paper is organized as follows: We describe our lattice model in Sec. II. Sec. III provides information about the simulation and analysis methods. This section is aimed at readers who are interested in the important but more technical details of our MC study and might be skipped by those readers interested only in the results, which we present in Sec. IV. Finally, in Sec. V, we summarize and make some concluding remarks.

II. MODEL

The aim of this paper is to investigate, by means of computer simulations, the phase behaviour of colloids immersed in a near-critical binary solvent. However, simulations of colloids in a molecular solvent with a bulk correlation length that diverges upon approaching the critical point pose major challenges from a computational point of view, as very different length- and time-scales are involved. Moreover two steps precede our investigations of the colloid-solvent model, (i) determining the phase diagram (binodal) and the critical point of the pure solvent and (ii) obtaining a good understanding of the behaviour of the solvent adsorbed on the surface of a single model colloidal particle (interfacial properties). It is therefore highly advantageous to choose a model for which the bulk phase diagram and interfacial properties have been established already or can be carefully investigated. To describe the solvent, we choose an incompressible nearest-neighbour *AB* lattice model which is isomorphic to the well known lattice-gas model of fluids. From a computational standpoint, lattice-based models are highly favourable since they are easy to parallelize and are computationally highly efficient. The lattice-gas model has been used extensively to study wetting and capillary phenomena, and the effects of confinement between planar walls.^{38,39} By drawing analogies directly between a binary solvent mixture and a one-component gas-liquid system with regard to phenomena such as complete wetting, capillary condensation, and critical adsorption,⁴⁰ we are provided with a wealth of information on interfacial properties pertinent to our solvent mixture.

Upon approaching the critical point of the solvent, it is important to simulate sufficiently large systems to accommodate the diverging correlation length.⁴¹ A direct consequence of the diverging correlation length is the critical slowing down

of the dynamics. It thus becomes increasingly difficult to simulate fluids as their critical point is approached, although algorithms exist which try to alleviate these problems by operating on correlated clusters.^{42,43} The size asymmetry (big colloid versus small solvent molecule) in our system is also a serious computational challenge. These complications forced us to restrict the present study to two-dimensional systems.

Thus, in our model of the solvent-colloid mixture, colloids are modelled as hard disks whose centres can undergo translational motion restricted to an underlying (solvent) lattice. The solvent and colloids also interact via nearest-neighbour interactions. Essentially, our model is an incompressible *ABC* mixture on a 2D square lattice, and shares many similarities with the lattice model used by Rabani *et al.*, to simulate the drying-mediated self-assembly of nanoparticles.⁴⁴ Our model also derives inspiration from the “finely discretized” lattice model of Panagiotopoulos.^{45,46} To elaborate, colloids *C* are discretized hard disks (HD) with a radius R , measured in number of lattice sites, and occupy a set of sites $S_C = \{r_i \mid d(r_i, r_C) \leq R\}$, where r_C are the lattice coordinates of the disk, r_i are the coordinates of lattice site i , and the function $d(a, b)$ calculates the absolute distance between a and b using the minimum image convention. The disks have only translational degrees of freedom, and their Hamiltonian H_C (in the absence of the solvent mixture) is zero for non-overlapping configurations, and is infinite if any pair of colloids overlap, or if a colloid and solvent site overlap. We assign to every lattice site i an occupancy number $n_i \in \{0, 1\}$. A lattice site i is occupied by a colloidal disk, and thus not available for a solvent species *A* or *B*, in the case $n_i = 1$. For occupancy number $n_i = 0$, lattice site i is not occupied by a colloidal disk and we assign an occupancy number $s_i \in \{-1, 1\}$ which indicates if it is occupied by solvent species *A* or *B*, respectively. We consider only nearest neighbour interactions and assign an energy penalty $\epsilon/2 > 0$ for every nearest neighbour *AB* pair, to drive *AB* demixing at sufficiently low temperatures, and an energy gain of $-\alpha\epsilon/2$ with $\alpha \geq 0$ for every *BC* pair, to mimic preferential adsorption of solvent *B* on the colloid surfaces. The parameter α measures the wettability of the colloidal disk. Fig. 2 illustrates the model.

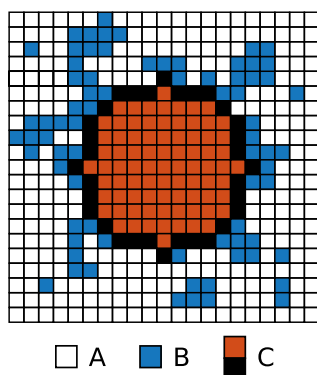


FIG. 2. A schematic representation of the colloid-solvent model with the grid representing the lattice sites. White cells are occupied by solvent species *A* and blue cells by solvent species *B*. The brown (interior) and black cells belong to a single colloidal particle, *C*, of radius $R = 6$. Particles of species *B* adjoining the black cells experience an attractive interaction of strength $\alpha\epsilon$.

The total Hamiltonian reads

$$H = H_C + \frac{\epsilon}{4} \sum_{\langle i, j \rangle} (1 - s_i s_j)(1 - n_i)(1 - n_j) - \frac{\alpha\epsilon}{4} \sum_{\langle i, j \rangle} n_i(1 + s_j)(1 - n_j), \quad (1)$$

where the summation runs over the set of distinct nearest neighbour pairs $\langle i, j \rangle$. In the absence of colloids, the *ABC* model reduces to the simple lattice-gas, or *AB* model.

III. METHODS

In order to study the structure and phase behaviour of the *ABC* model of a binary solvent-colloid mixture, just described, we choose to use Monte Carlo simulations. To this end, the following Monte Carlo moves are employed:

- An attempt to flip the solvent occupancy s_i of every site, i.e., sites which have $n_i = 0$.
- An attempt to translate every colloidal particle in the system, along either the x or y axis.

The occupancy flip moves are accepted using the standard Metropolis criterion for changing the number, N_B , of sites occupied by *B*,

$$a(N_B \rightarrow N_B \pm 1) = \min \left[1, e^{-\beta(\Delta E \mp \epsilon \Delta \mu_s)} \right], \quad (2)$$

with ΔE the difference in potential energy (Hamiltonian Eq. (1)) of the new and old configuration. The dimensionless quantity $\Delta \mu_s = (\mu_B - \mu_A)/\epsilon$ denotes the chemical potential difference of solvent species *A* and *B*, and $\beta = 1/k_B T$ is the inverse temperature, with k_B Boltzmann’s constant. Note that the acceptance rule (2) depends on the chemical potential difference $\Delta \mu_s$ as the total number of solvent species $N_s = N_A + N_B$ is fixed, and thus $N_B \rightarrow N_B + 1$ simultaneously means that $N_A \rightarrow N_A - 1$. Disk translations are handled using symmetry operations⁴² to remove any disk-solvent overlaps. An attempt is made to move a disk in a random direction x or y by one lattice site. If no overlaps with other disks occur, the disk is translated and the sites outlined with a green colour in Figure 3 are reflected with respect to the new disk position. The move is then accepted using the Metropolis algorithm.

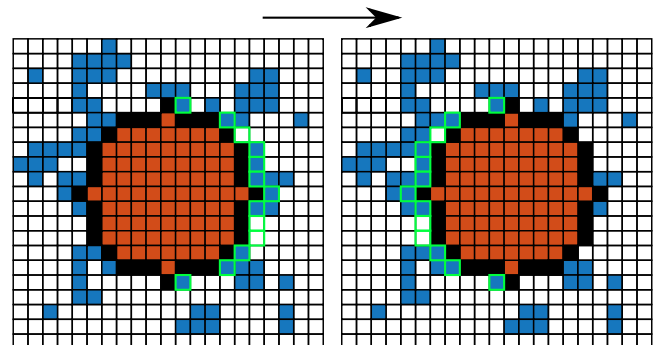


FIG. 3. Illustration of the translation of a colloid. Here we attempt to move the disk by one lattice site to the right. Any site that is occupied by solvent species *B* (blue outlined with green colour) is reflected with respect to the new disk position, resulting in the new configuration seen in the right figure.

To determine the phase behaviour, we use the direct interfacial or coexistence simulation method⁴⁷ in combination with the grand-canonical staged-insertion (GCSI) Monte Carlo technique.^{48–50} In spite of the simplicity of our model, a considerable amount of computational time is needed to collect data with sufficiently high accuracy. Below, we describe these techniques, tailored for the *ABC* model, in more detail.

A. Direct coexistence simulations

In the direct coexistence method, simulations are performed in the canonical ensemble at a thermodynamic state point that lies well inside the two-phase coexistence region of the ternary mixture. The system will therefore phase separate according to the lever rule. To facilitate the formation and subsequent stabilization of the interfaces between the two phases, an elongated simulation box with a typical aspect ratio of 2:1 is chosen. The densities of the coexisting phases can then be computed from the density profiles of the system. The direct interfacial simulation is computationally the least expensive method for determining phase coexistence when compared to alternative techniques. However, the method has several disadvantages: for finite-sized systems a significant fraction of particles are at or near the interface, and when a critical point is approached, the interface becomes very broad as the surface tension approaches zero. Therefore the simulations become inaccurate close to the critical point of the ternary *ABC* mixture.

For our *ABC* model, we utilize this technique to determine gas-solid coexistence since alternative techniques that involve particle insertions, e.g., grand canonical or Gibbs ensemble Monte Carlo simulations, are not feasible in the case of crystal phases. In our direct coexistence simulations we treat the colloids canonically while the solvent is treated grand canonically, i.e., we fix the number of colloids N_C , the solvent chemical potential difference $\Delta\mu_s$, the volume V (or area, in the present case) of the system, and the temperature T . At fixed $\Delta\mu_s$ and reduced temperature τ , we run simulations at a series of colloid packing fractions, η . If the value of η lies between two bulk coexisting density values, phase coexistence is observed directly in the simulations. We can then estimate the densities of the coexisting phases from the average density profiles of the system in the direction perpendicular to the interface.

B. Grand canonical staged-insertion method

In order to get accurate estimates of the colloidal gas-liquid coexistence region of the phase diagram we perform grand canonical simulations, i.e., we fix $\Delta\mu_s, V, T$, and the colloid chemical potential difference, $\Delta\mu_c = (\mu_c - \mu_{Av_c})/\epsilon$, with μ_c the chemical potential of the colloids and v_c the number of lattice sites occupied by a single colloidal particle. Simulations in the grand canonical ensemble involve additional Monte Carlo moves which attempt to either insert or remove colloidal hard disks from the system. Due to the size asymmetry between the colloids (*C*) and the solvent species, and the hard-core repulsion between the hard disks,

the acceptance of such moves becomes prohibitively low. Recently, a technique which deals effectively with this issue was introduced by Ashton and Wilding.⁴⁸ This is based on the expanded ensemble simulation technique, see Refs. 49 and 50 for more details. Next, we describe the implementation of this method, called grand canonical staged-insertion (GCSI), for our *ABC* model.

The grand canonical partition function of the ternary system can be written as

$$\Xi = \sum_{\{\Omega\}} e^{-\beta(H - \epsilon\Delta\mu_s N_B - \epsilon\Delta\mu_c N_C)}, \quad (3)$$

where $\{\Omega\}$ is the set of all allowed configurations of the lattice, N_C is the number of colloids. Due to the symmetries present in our model, the ternary *ABC* system is equivalent to a binary system where the amount of species *B* and *C* is controlled by fields $\Delta\mu_s$ and $\Delta\mu_c$, respectively. The staged insertion method involves inserting the colloidal (large) particle in stages. That is, one could insert a small particle and grow it to the desired size, or insert an ideal-gas particle of the desired size and couple it to the system energetically in a series of stages. We use the latter method, and refer to the particle inserted in stages as the ghost particle. In principle there is no restriction on the number of ghost particles in the system, however, we employ a maximum of one ghost particle at any instant of the simulation.

A ghost particle can transition between M different stages, where stage $m = 0$ is equivalent to a system of N_C colloidal particles and $m = M - 1$ is equivalent to a system with $N_C + 1$ colloidal particles. The ghost particle at a particular stage m interacts with the solvent particle in the following fashion: at stage $m = 0$ the ghost particle is merely an ideal gas particle, with no interaction with the solvent particles, and at $m = M - 1$, the solvent particles at the surface of the colloid interact with an attractive interaction of strength α , and solvent particles existing within the hard core experience an infinite repulsion. Following Ashton and Wilding⁴⁸ we introduce a stepwise potential for the intermediate stages. The ghost particle has an m -dependent field strength α_m and an additional field, with strength σ_m , associated with the excluded-volume interaction of the ghost particle with the solvent sites. A typical set of stage-dependent fields used in our simulations is

$$\alpha_m = \alpha \frac{m}{M-1}, \quad (4)$$

$$\sigma_m = \frac{m}{M-1-m},$$

where we typically employ $M = 6$ stages. Depending on the simulated state point, different forms of the fields α_m and σ_m can provide better acceptance rates. The method increases slowly the coupling of the ghost particle to the system by interpolating the two fields, between the fully coupled and fully decoupled state.

The partition function of the system with the inclusion of a ghost particle is given by

$$\Xi_m = \sum_{\{\Omega_m\}} e^{-\beta(H + H_m^G - \epsilon\Delta\mu_s N_B - \epsilon\Delta\mu_c N_C)}, \quad (5)$$

where $\{\Omega_m\}$ is the set of all allowed configurations including a ghost particle at stage m , and H_m^G is the interaction Hamiltonian of the ghost particle at stage m ,

$$H_m^G = -\frac{\alpha_m \epsilon}{4} \sum_{\langle i,j \rangle} g_i(1+s_j)(1-g_j) + \frac{\sigma_m \epsilon}{2} \sum_i g_i(1+s_i), \quad (6)$$

where $g_i \in \{0,1\}$ denotes the presence of a ghost particle at lattice site i . Note that the grand canonical ensemble is a subset of the above ensemble. More specifically, this is the subset

for which the stage index $m = 0$. The expanded ensemble partition function, is then simply defined as the sum of Ξ_m over the different stages, m ,

$$\Xi_E = \sum_{m=0}^{M-2} \Xi_m. \quad (7)$$

To simulate the system in the expanded ensemble, a Monte Carlo move is introduced which attempts to change the stage index, as shown in Figure 4. The move is accepted using the Metropolis criterion with a probability given by

$$a(\{N_C, M-2\} \rightarrow \{N_C+1, 0\}) = \min(1, \exp\{-\beta(U_0^G - U_{M-2}^G) + \beta\epsilon\Delta\mu_c - \ln(N_C+1)\}), \quad (8)$$

$$a(\{N_C, 0\} \rightarrow \{N_C-1, M-2\}) = \min(1, \exp\{-\beta(U_{M-2}^G - U_0^G) - \beta\epsilon\Delta\mu_c + \ln N_C\}), \quad (9)$$

$$a(\{N_C, m\} \rightarrow \{N_C, m \pm 1\}) = \min(1, \exp\{-\beta(U_{m \pm 1}^G - U_m^G)\}), \quad (10)$$

where U_m^G is the potential energy due to the interactions with the ghost at stage m , given by Equation (6). During each sweep we perform k such moves. After every move, we equilibrate locally the solvent sites in a square of size $(2R+3) \times (2R+3)$ centred around the position of the ghost particle, to facilitate the transition between stages.

C. Transition matrix Monte Carlo technique

As we mentioned earlier, the interface of the ternary mixture in the two-phase region becomes too diffuse for us to make reliable measurements close to the critical point using direct coexistence simulations. In order to determine the accurate phase coexistence in this case, we use the transition matrix Monte Carlo (TMCM) technique to calculate the particle number probability distribution $P(N_C)$ in a grand canonical Monte Carlo simulation. The objective of the TMCM technique is to estimate the probability of observing the system at a certain value of a chosen macrostate variable, Y , i.e., energy, volume, and density. We employ this technique to determine phase coexistence but also the probability distribution of the distance between two colloids, $P(\mathbf{r})$, from which the effective colloid-colloid potential can be calculated.

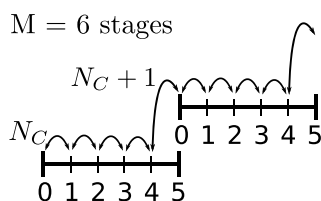


FIG. 4. Allowable transitions for a ghost particle with $M=6$ stages. Note that a system with N_C colloids and a ghost at stage index $m = M-1$ (5 in the diagram), the stage at which the ghost becomes fully coupled, is equivalent to a system with N_C+1 colloids and a ghost at stage index $m=0$, where the ghost is fully decoupled.

The TMCM technique is also used to determine the probability distribution of the number of BC surface interactions, m_B , around a colloid, $P(m_B, \alpha)$. This enables us to calculate the saturation point for the colloid wettability, α , i.e., the value at which the colloid has essentially only species B solvent neighbours.

A TMCM simulation involves a regular simulation of the system with a few additional bookkeeping steps. After every move which attempts to change the macrostate, Y , of the system, regardless of whether the move is accepted, we update a collection matrix in the following fashion:

$$C(Y \rightarrow Y') = C(Y \rightarrow Y') + a(y \rightarrow y'), \quad (11)$$

$$C(Y \rightarrow Y) = C(Y \rightarrow Y) + 1 - a(y \rightarrow y'),$$

where the lower-case y denotes the microstate variable corresponding to the observed macrostate variable, Y . Periodically during the simulation the macrostate transition probability $\pi(Y \rightarrow Y')$ is estimated as follows:

$$\pi(Y \rightarrow Y') = \frac{C(Y \rightarrow Y')}{\sum_W C(Y \rightarrow W)}. \quad (12)$$

If we restrict transitions such that any macrostate has only two neighbouring macrostates, and provided the transition probabilities are estimated, the macrostate probabilities $P(Y)$ can be calculated simply using the detailed balance condition,

$$P(Y)\pi(Y \rightarrow Y') = P(Y')\pi(Y' \rightarrow Y). \quad (13)$$

In order to sample efficiently all macrostates, the acceptance probabilities are biased according to the multicanonical approach in the following fashion:

$$a_b(y \rightarrow y') = \min(1, e^{\eta(Y') - \eta(Y)} a(y \rightarrow y')), \quad (14)$$

where $\eta(Y) = -\ln P(Y)$. We begin initially with a flat distribution for $\eta(Y)$. Then routinely as $P(Y)$ is estimated, we update the biasing function and the simulations are

continued until the distribution $P(Y)$ converges within a certain acceptable tolerance.

In the grand canonical ensemble, knowledge of the particle number probability distribution, $P(N)$, allows one to calculate easily the densities of the two coexisting phases using histogram reweighting techniques.⁵¹ For the GCSI simulations, we associate the macrostate variable Y , with the pair $\{N_C, m\}$. The dimension of the collection matrix is $(N_C^{max} \times M - 1) \times (N_C^{max} \times M - 1)$. In order to improve the efficiency of the method we split the range $[0, N_C^{max}] \times [0, M - 1]$ into several overlapping windows of size $[N_C^i, N_C^{i+1}] \times [0, M - 1]$, and simulate the windows in parallel. The macrostate probabilities, $P(Y)$, are then estimated by combining the probabilities from each window in the following manner:

$$\log P(Y_i) = \log P(Y_{I(i)}^{W(i)}) + \sum_{j=0}^{W(i)-1} \log P(Y_{n_j}^j), \quad (15)$$

where Y_i is the i th macrostate, Y_i^j is the i th macrostate of window j , and the functions $W(i)$ and $I(i)$ give the window, and index inside the window of macrostate i , respectively. $Y_{n_i}^i$ is the last macrostate of window i , and $Y_{n_i}^i = Y_0^{i+1}$. Note that when $Y_i = Y_{n_j}^j = Y_0^{j+1}$, then $W(i) = j + 1$, and $I(i) = 0$. The particle number probability distribution, $P(N_C)$, then follows directly from $P(\{N_C, m\})$, by setting $m = 0$.

In calculating the two-body effective interaction, $U(\mathbf{r})$, one particle is kept immobile at position $\mathbf{r} = (0, 0)$, while the position of the second is used as the macrostate variable for the transition matrix. This allows us to calculate the effective interaction between a pair of colloids as, $\beta U(\mathbf{r}) = -\ln[P(\mathbf{r})/P(\mathbf{r} \rightarrow \infty)]$. As the particle is only allowed to translate to the nearest lattice sites, the problem of calculating the macrostate probabilities can be described as a quasi-birth-death process.^{52,53} In order to calculate the probabilities $P(\mathbf{r})$, instead of Equation (12), we solve the global balance equation which in matrix notation can be written as

$$\mathbf{P} = \boldsymbol{\pi} \mathbf{P}. \quad (16)$$

The above equation can be solved easily using an iterative solver such as successive over-relaxation, if we rewrite it as

$$\mathbf{P}^{i+1} = \boldsymbol{\pi} \mathbf{P}^i \quad (17)$$

with the index i denoting the i th iteration of the algorithm.

Using the simulation methods described above, we study the phase behaviour and structure of a 2D lattice model of discretized colloidal hard disks in a near-critical binary solvent mixture. In addition, we investigate systematically the effects of wettability, α , and the colloid radius, R , on the phase behaviour of the model colloidal suspension.

IV. RESULTS

A. Phase diagram of solvent

In the absence of colloids, the AB solvent is isomorphic to the Ising model and in 2D the exact phase diagram is known analytically from Onsager.⁵⁴ In Figure 1 we represent the phase diagram of the solvent in τ vs. x_r representation, where

$\tau = (T - T_c)/T_c$ is the reduced temperature, with T_c the critical temperature of the pure solvent, and x_r , the composition. The critical temperature is given by $k_B T_c = 0.567\epsilon$. We use the subscript r to denote the solvent reservoir. Due to the Ising symmetry inherent to the AB lattice model, the critical composition $x_{r,c} = 1/2$ and the chemical potential corresponding to the binodal, at which saturation occurs, is at $\Delta\mu_s = 0$, for $\tau < 0$. For $\Delta\mu_s < 0$ ($\Delta\mu_s > 0$) the bulk solvent mixture is rich in solvent species A (B). In this paper we show results for colloids which prefer the B species of the supercritical solvent.

It is important to comment on the choice of our model. Had we chosen a different model, lattice or off-lattice, to describe the solvent, we would have needed to compute and identify with great accuracy the solvent phase diagram. Moreover, given that a grand canonical treatment of the solvent is the most accurate way to study the phase behaviour of the ABC model, lattice models offer computational advantages over off-lattice models.

B. Adsorption at a single wall

Before we present our results on the phase behaviour of colloids, we study first the adsorption behaviour of the solvent mixture at a flat planar wall, which can be regarded as an infinitely large colloid. We consider only nearest neighbour interactions between solvent species B and the wall. As described in Section II, the wettability parameter, α , is a measure of the preference of the substrate for solvent species B . For $\alpha = 0$, the planar wall prefers neither solvent species and is termed neutral. For such a wall, and $\Delta\mu_s = 0$, there is no ordering at the surface,⁵⁵ due to the perfect AB (Ising) symmetry.

In this work we consider only states where the solvent is super-critical, i.e., $\tau > 0$, and surfaces with wettability $\alpha > 0$. In the limit $\tau \rightarrow 0^+$, the solvent exhibits critical adsorption, i.e., the thickness of the adsorbed film is determined by ξ , the bulk correlation length of the solvent.² Thus, as the critical point is approached, the presence of a wall can be felt at very large distances, set by the diverging ξ . In Figure 5 we present

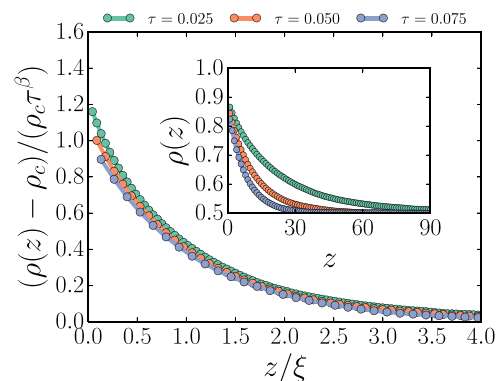


FIG. 5. Density profiles of species B adsorbed on a planar wall with wettability $\alpha = 0.6$, for $\Delta\mu_s = 0$, and three reduced temperatures τ . In the main figure, the distance from the wall z is scaled with the correlation length of the pure solvent $\xi = 0.567\tau^{-1}$. The inset shows the unscaled profiles. ρ_c is the critical density.

the density profiles of species B adsorbed on a planar wall with $\alpha = 0.6$, at reduced temperatures, $\tau = 0.025, 0.05$, and 0.075 , for $\Delta\mu_s = 0$, i.e., at fixed critical composition. $\rho(z)$ is simply the local composition at distance z from the planar wall, with z measured in lattice spacings. The critical density, $\rho_c = \rho(\infty)$, is the critical composition, i.e., $\rho_c = x_{r,c} = 1/2$. We choose to use the term density profile since this makes clear the connection with studies of real (off-lattice) mixtures. The scaling in Figure 5 is motivated by general considerations.² Distances from the wall are scaled with ξ , the bulk correlation length, and the deviation from the critical density is scaled by $\tau^{-\beta}$, where the order parameter critical exponent $\beta = 1/8$ in $D = 2$. The plot demonstrates excellent data collapse to the universal scaling prediction and confirms that the simulations can tackle efficaciously near-critical adsorption phenomena. Note that the scaling described in Figure 5 is applicable only for $\Delta\mu_s = 0$. For non-zero values of $\Delta\mu_s$ a field (chemical-potential) dependent variable enters the scaling relation.

The thickness of adsorbed films is highly sensitive to the thermodynamic state of the solvent reservoir. Thick adsorbed films are also observed far from the critical point of the solvent. In particular, these can arise for $\tau < 0$ when wetting films develop. We refer to adsorption far from the critical scaling regime as preferential adsorption; this is a non-universal phenomenon. Here the detailed nature of the wall-fluid interactions plays a key role in determining the film thickness, and hence the effective interactions between colloidal particles suspended in the solvent.

C. Neutral vs. attractive colloids

We now turn our attention to a system of many colloids immersed in a supercritical binary solvent mixture, $\tau > 0$, and relatively poor in the colloid-preferred species B , $\Delta\mu_s \leq 0$, i.e., we consider states corresponding to those in the hatched region in Figure 1. This choice precludes solvent-mediated colloidal aggregation arising from complete wetting and capillary condensation, i.e., formation of capillary bridges.⁵⁶ To this end, we consider a colloidal suspension at a fixed packing fraction η (the fraction of lattice sites occupied by colloids), and we treat the solvent grand-canonically, i.e., we view our system as being in thermal and diffusive contact with an AB solvent reservoir with composition x_r that fixes τ and $\Delta\mu_s$. Generally, the ABC mixture has composition $x \neq x_r$. Here x denotes the fraction of sites occupied by B when the colloids are present. Note that the variable τ merely sets the temperature of the reservoir and is not a measure of distance from criticality of the ternary mixture. We consider first the case of neutral colloids of radius $R = 6$, which have no preference for species A or B ($\alpha = 0$). In Fig. 6 (Top) we show a system of these colloids (right) at $\tau = 0.005$ and $\Delta\mu_s = 0$ in equilibrium with the solvent reservoir (left). The visualization reveals the tendency of the colloids to preferentially adsorb at the ‘interfaces’ between the instantaneous (*supercritical*) A and B domains. This feature, which resembles the binding of colloids to static air-liquid or liquid-liquid interfaces by a Pieranski potential,⁵⁷ is captured here owing to the Brownian character of the colloids. Fig. 6 (Bottom) shows a visualization for the same parameter set, except now the colloids strongly

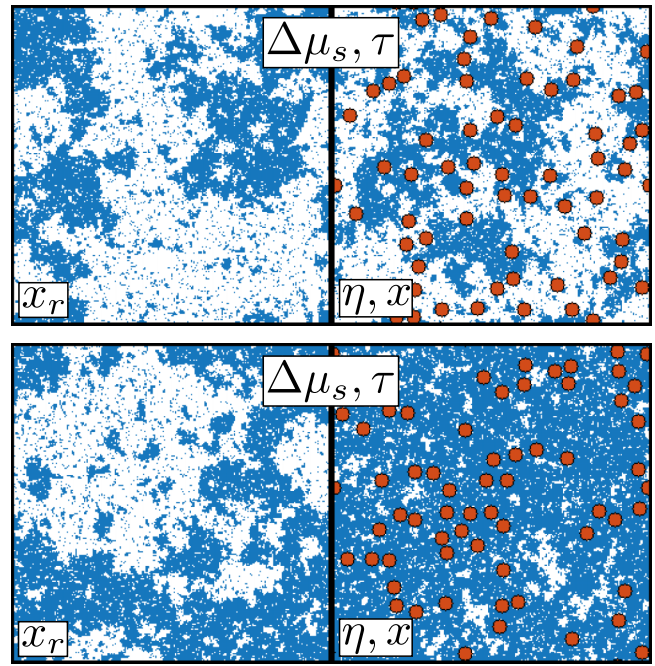


FIG. 6. **Top:** Typical configurations of a ternary ABC mixture (right) with neutral colloids with no preference for A or B (radius $R=6$, $\alpha=0$) at colloid packing fraction $\eta=0.11$ and solvent composition $x=(1-\eta)/2$ in equilibrium with a solvent reservoir (left) with $\eta=0$, $\Delta\mu_s=0$, $x_r=1/2$, $\tau=0.005$, and bulk correlation length $\xi \approx 19R$. **Bottom:** Typical configurations of a ternary ABC mixture (right) with colloids strongly preferring solvent B ($R=6$, $\alpha=19.0$) at packing fraction $\eta=0.11$ and solvent composition $x > (1-\eta)/2$ in equilibrium with the same solvent reservoir (left) as in **Top**. The system consists of 512×512 lattice sites and in both the **Top**, and **Bottom**, the number of colloids is $N_C = 64$.

prefer solvent B ($\alpha = 19$). The strong B -adsorption on the colloids and the unfavourable AB interaction lead to an overall excess of B , thereby driving the ABC mixture far away from criticality; the solvent correlation length is observed to be smaller than the particle size. This is in sharp contrast to Fig. 6 (Top) where the correlation length of the solvent is hardly altered by the presence of neutral colloids.

D. Phase behaviour and structure

The results in Subsection IV C refer to $\Delta\mu_s = 0$. Here we focus on $\Delta\mu_s < 0$ where colloidal phase transitions occur. As mentioned earlier, due to the symmetries inherent in our model, the ternary ABC mixture is equivalent to a binary mixture and therefore any binodals are a two-dimensional manifold in the three-dimensional η vs. $\Delta\mu_s$ vs. τ space. We determine cuts of this manifold at certain fixed temperatures. Here, we expand upon key results from our earlier work on the ABC model.¹

Once again, we fix the parameters $R = 6$ and $\alpha = 0.6$, and determine the binodals at three different fixed temperatures $\tau = 0.025, 0.05$, and 0.075 , as shown in Figure 7. We choose these temperatures as the bulk correlation length, $\xi = 0.567/\tau$, of the solvent reservoir evaluated at $\Delta\mu_s = 0$, is then comparable to the size of the colloid. We plot the binodals in the η vs. $\Delta\mu_s$ representation. In this representation the tie-lines are horizontal. We observed stable colloidal gas (G), liquid (L), and crystal (X) phases.¹ There is broad

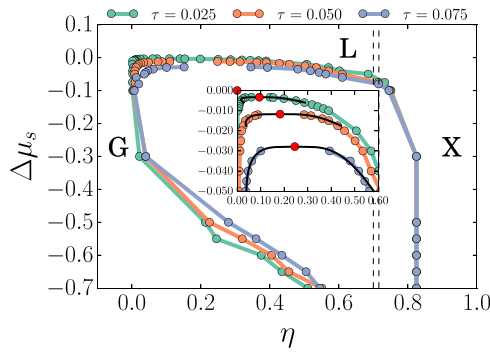


FIG. 7. Binodals of the *ABC* ternary mixture, computed using a combination of the GCSI-TMMC method for near-critical $\Delta\mu_s$, and the direct coexistence method for the remaining points, for three fixed temperatures $\tau = 0.025$ (green), $\tau = 0.05$ (orange), and $\tau = 0.075$ (blue) with $R = 6$ and $\alpha = 0.6$. In this solvent chemical potential, $\Delta\mu_s$, vs. colloid packing fraction, η , representation, the tie lines are horizontal. The red circles and black lines in the inset are the critical points and binodals obtained by least-squares fitting of Equation (18). Note that the vertical dashed lines denote fluid-solid coexistence for pure hard disks. This plot reproduces the data in Fig. 3 of Ref. 1 and now incorporates the fitting to Eq. (18).

G-X coexistence for $\Delta\mu_s < -0.1$. The vertical dashed lines in Figure 7 correspond to the (discretized) hard-disk phase behaviour that is recovered in the limit $\Delta\mu_s = \pm\infty$.^{1,37} In the inset to Figure 7 we have also plotted estimates of the critical points, obtained by a least-squares fit to the equation,^{58–61}

$$\eta_{\pm} - \eta_c = A |\Delta\mu_s - \Delta\mu_s^c| \pm \frac{1}{2} B |\Delta\mu_s - \Delta\mu_s^c|^{\beta} \quad (18)$$

where η_{\pm} stands for colloidal liquid/gas packing fraction, with η_c its critical value, and A and B , as well as the exponent, β , are fit parameters. Note that we have substituted temperature with the solvent chemical potential, $\Delta\mu_s$, with $\Delta\mu_s^c$ being the solvent chemical potential at the critical point of the ternary mixture. It is important to realize that Equation (18) is not an exact relation, and under this understanding, we fit it to our results mostly as a guide to the eye.

In the remainder of this work we shall focus on the G-L coexistence. In Figure 8 we show a visualization of G-L coexistence for $\tau = 0.05$ and $\Delta\mu_s = -0.04$. We note the presence of two G-L interfaces and that the composition of the solvent in the coexisting phases is very different. The liquid phase, *L*, dense in colloids (orange disks), is extremely dilute in species *A* (white). By contrast, the gas phase, *G*, dilute

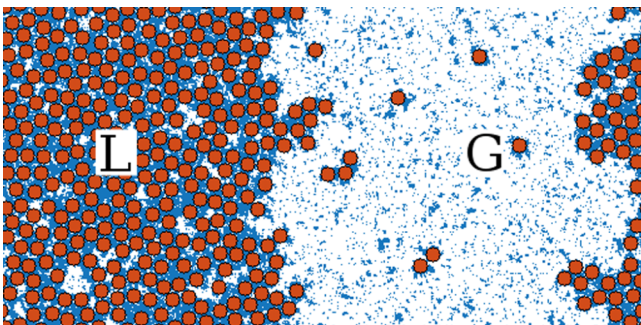


FIG. 8. Simulation snapshot of a system of 256×512 lattice sites and 348 colloids with $R = 6$ and $\alpha = 0.6$, at $\tau = 0.05$, showing gas-liquid (G-L) coexistence at $\Delta\mu_s = -0.04$.

in colloids, is rich in *A*. Indeed, the solvent composition in *G* is close to that of the reservoir: $x \approx x_r$. This is important to note as several theoretical approaches that study the phase behaviour of a colloid solvent mixture treat the solvent as a uniform background with a fixed composition in both the coexisting phases.^{11–13,36}

The G-L coexistence shown in Figure 7 terminates at a critical point (see red circles) that shifts to lower $\Delta\mu_s$ and higher packing fraction, η , with increasing τ . A signature of criticality is the divergence of the partial structure factors, $S_{ab}(k)$, in the low k limit. We note that in any mixture, the solvent-solvent ($ab = BB$), colloid-colloid ($ab = CC$), and solvent-colloid ($ab = BC$) pair correlation functions should all decay with the same true correlation length.⁶² Calculations of $S_{BB}(k \rightarrow 0)$ vs. η yield a rough estimate of the G-L critical point. In Figure 9(a) we show the *BB* structure factor defined as $S_{BB}(k) = (1/N) \langle n_{\mathbf{k}}^B n_{-\mathbf{k}}^B \rangle$, where $n_{\mathbf{k}}^B$ is the Fourier transform of the solvent species *B* occupancy profile.⁶³ We compute $S_{BB}(k)$ at $\tau = 0.025$ and $\Delta\mu_s = -0.00315$ and five values of η , i.e., the state points indicated by dots in the phase diagram shown in the inset of Fig. 9(a). In Fig. 9(b) we plot the limit $S_{BB}(k \rightarrow 0)$, obtained from a linear extrapolation to $k = 0$ of the simulation data, vs. η . This shows a maximum corresponding to the state closest to the G-L critical point. Fig. 9(a) displays data for two values of η (0.1724 and 0.3276) for which $S_{BB}(k)$ exhibits pronounced oscillations.

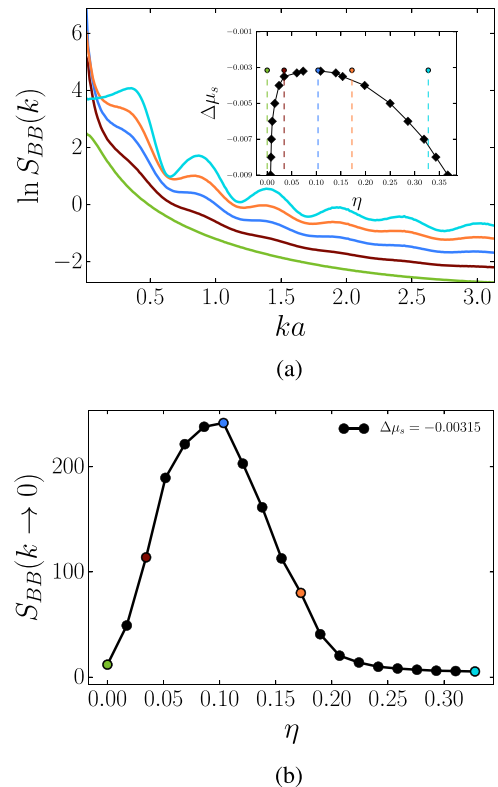


FIG. 9. (a) Partial structure factor, $S_{BB}(k)$, of the solvent computed at $\tau = 0.025$, $\Delta\mu_s = -0.00315$, $R = 6$, at different values of colloid packing fraction: $\eta = 0.0$ (green), $\eta = 0.0345$ (brown), $\eta = 0.1035$ (blue), $\eta = 0.1724$ (orange), and $\eta = 0.3276$ (cyan). For clarity, the curves were shifted by 0.5 on the log-scale. The inset shows the G-L binodal for $\tau = 0.025$ (black diamond symbols). (b) The value of the structure factor linearly interpolated to $k = 0$, $S_{BB}(k \rightarrow 0)$ vs. η , at $\Delta\mu_s = -0.00315$.

The period of these is about $\Delta k \approx 0.54/a$, with a the lattice spacing, which implies that the wavelength of oscillations in $g_{BB}(r)$ is about $12a$, the diameter of the colloidal hard disks. Examination of plots of $g_{ab}(r)$ (see Fig. S3 of Ref. 1) shows that all three oscillate with roughly this wavelength. In other words, the (large) colloidal length scale determines the form of BB and BC correlations, as well as CC correlations, at sufficiently large packing fraction η .

1. Phase behaviour: Dependence on α

Here we discuss how the phase behaviour of the model depends on the wettability α of the colloids C . Recall that values of $\alpha > 0$ cause species B to preferentially adsorb on the surface of colloid C . We have shown that phase separation into colloidal gas, liquid, or crystal phases then occurs for $\Delta\mu_s < 0$, i.e., where the bulk solvent reservoir is rich in species A . Clearly, the phase separation is driven by a competition between bulk, favouring A , and colloid adsorption, favouring B . When $\Delta\mu_s > 0$, so that the bulk reservoir is rich in species B , there is no phase separation. By the same argument, if we set $\alpha < 0$, then phase separation will be observed for states where the bulk prefers species B , i.e., $\Delta\mu_s > 0$.

The role of α in our model is to promote the formation of an adsorption layer around each colloidal particle. This extends, due to solvent-solvent correlations, up to a distance given by the solvent correlation length ξ . Above a certain value of α the surface of the colloid remains saturated with particles of species B . In Figure 10 we show m_B , the fraction of BC interactions on a single colloidal particle, as a function of the wettability, α , for reduced temperature $\tau = 0.025$, and $\Delta\mu_s = 0$ and -0.1 . As expected, for $\Delta\mu_s = 0$, $m_B = 1/2$ for the neutral case $\alpha = 0$. These results are obtained by calculating the probability $P(m_B; \alpha)$ using TMMC (see Section III C), and subsequently using histogram reweighting in the wettability, α . This procedure is similar to that described in Ref. 64. From Figure 10 we see that the surface layer is saturated at $\alpha \approx 3$.

In Figure 11 we plot the G-L coexistence region of the phase diagram for four different values of the wettability α at a fixed temperature $\tau = 0.025$ and colloid radius $R = 6$. The binodals are computed from probability distributions using the TMMC technique (see Section III C) for a system size $L = 256$, and broaden upon increasing the wettability. However, for α beyond a saturation value of about 4.0, the

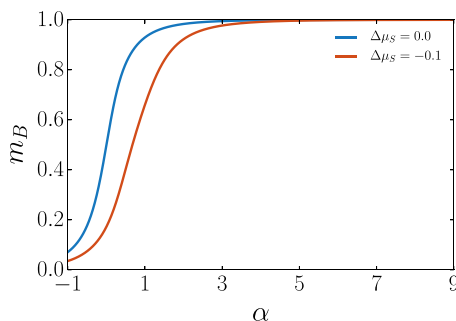


FIG. 10. Fraction of BC interactions, m_B , for a colloid of $R=6$, as a function of the wettability, α , at temperature $\tau=0.025$, for two different values of the solvent chemical potential, $\Delta\mu_s$.

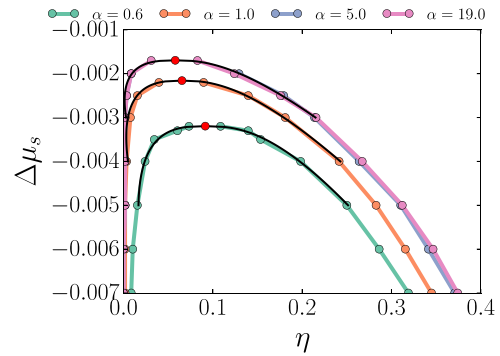


FIG. 11. G-L binodals for the full ABC ternary mixture plotted as hard-disk packing fraction η vs. solvent chemical potential $\Delta\mu_s$ for $\alpha=0.6$ (green), $\alpha=1.0$ (orange), $\alpha=5.0$ (blue), and $\alpha=19.0$ (pink). The temperature $\tau=0.025$ is fixed, and $R=6$. The red circles and black lines are the critical points and binodals obtained by least-squares fitting of Equation (18). Note that for $\alpha=5.0$ and 19.0 , the binodals are extremely close.

binodals are unchanged. Provided α is sufficiently large that the surface layer around the colloid is occupied fully by B , i.e., $m_B = 1$ in Fig. 10, G-L coexistence remains unaffected by stronger wettability. Note that for $\alpha = 0.6$, the value chosen for the majority of our studies, m_B is typically about 0.8–0.9 for states close to the colloidal critical points.

The results in Fig. 11 correspond to a much narrower range of $\Delta\mu_s$ than in Fig. 7. In addition to broadening the binodals, increasing α shifts the colloidal critical point to smaller values of η and to smaller values of $|\Delta\mu_s|$. This trend is similar to that found in the mean-field treatment of Edison *et al.* (see Fig. 7 of Ref. 37).

For $\Delta\mu_s < -0.1$, we observed broad G-X coexistence (not shown in Figure 11) similar to that shown in Figure 7. In this regime lattice effects become important and below we explain this in more detail.

2. Phase behaviour: Dependence on R

Next we discuss the dependence of the phase behaviour on the radius of the colloids, R . We computed the phase diagrams of three systems where the colloids have radii $R = 6$, $R = 9$, and $R = 12$. Ideally we would like to investigate colloid sizes which are much larger $\sim O(100)$. However, determining the phase behaviour of these systems using the aforementioned techniques is not computationally feasible. The sizes we investigate are more representative of nanoparticles in solvents than micron-sized colloids. The G-L binodals are computed from probability distributions using the TMMC technique (see Section III C). We used system sizes of $L = 256$, 384, and 512 for colloid radii $R = 6$, 9, and 12, respectively. In Figure 12 we show the G-L binodals at a fixed temperature $\tau = 0.025$. We set the wettability $\alpha = 0.6$ for all three cases. Increasing the radius broadens the binodal and shifts the colloidal critical point to larger values of η and smaller values of $|\Delta\mu_s|$. The same trend is found in Fig. 8 of Ref. 37. Note that for $R = 12$, the binodal is extremely flat in the neighbourhood of the critical point.

As a remark concerning the critical behaviour of the ternary mixture, we note that although the various liquid-gas coexistence curves in Figs. 11 and 12 appear to show different

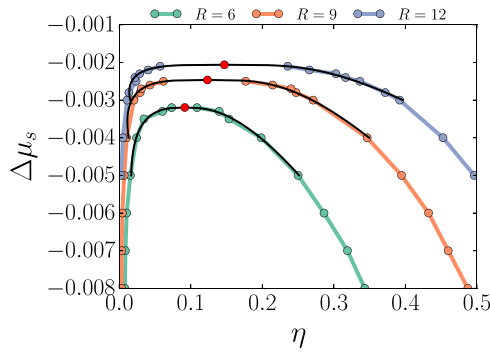


FIG. 12. G-L binodals for the full *ABC* ternary mixture plotted as hard-disk packing fraction η vs. solvent chemical potential $\Delta\mu_s$, for particle radius, $R=6$ (green), $R=9$ (orange), and $R=12$ (blue). The temperature is fixed at $\tau=0.025$ and wettability $\alpha=0.6$. The red circles and black lines are the critical points and binodals obtained by least-squares fitting of Equation (18).

degrees of “flatness” in the vicinity of their critical points, all the ternary mixtures must lie in the 2D Ising universality class. In other words, were we able to perform simulations for increasing system sizes at states sufficiently close to criticality, and employ finite-size scaling arguments, we would find the critical exponent in Eq. (18) is $\beta = 1/8$. Current resources do not permit such an analysis.

E. The effective two-body potential

In this subsection we present some results for the effective pair potential, $U(r)$, obtained from our MC simulations, using the method described in Section III C. The potentials shown in Figure 13, for $R=6$ and $\alpha=0.6$, are calculated at the solvent state points given in the inset, i.e., $\tau=0.025$ and three different values of $\Delta\mu_s$. For the state at the critical composition, $\Delta\mu_s=0$, the potential is slowly decaying. Recall that the correlation length $\xi \sim 23$ lattice spacings at this state point. For $\Delta\mu_s=-0.01$, slightly off the critical composition, the potential decays faster but the range is comparable with ξ . However, the minimum of $U(s)$, which occurs at

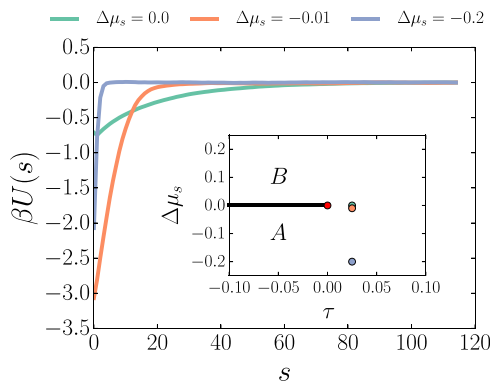
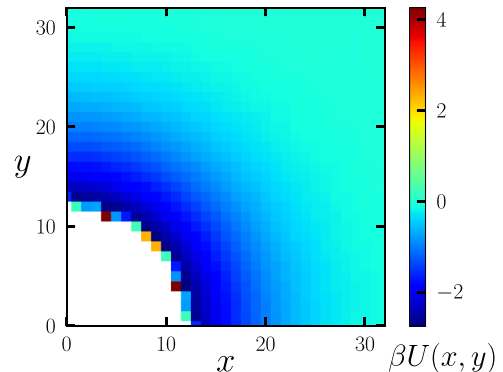


FIG. 13. Effective two-body potentials, $U(s)$, between two colloids of radius $R=6$ and $\alpha=0.6$, suspended in a solvent at $\tau=0.05$, for $\Delta\mu_s=0$ (green), $\Delta\mu_s=-0.01$ (orange), and $\Delta\mu_s=-0.2$ (blue). Here, s is the surface to surface distance, $s=|r^2-(2R+1)$. The inset shows the phase diagram of the *AB* solvent in the $\Delta\mu_s$ vs. τ representation. The red dot denotes the solvent critical point. The other dots show the state points at which the effective potential is calculated.

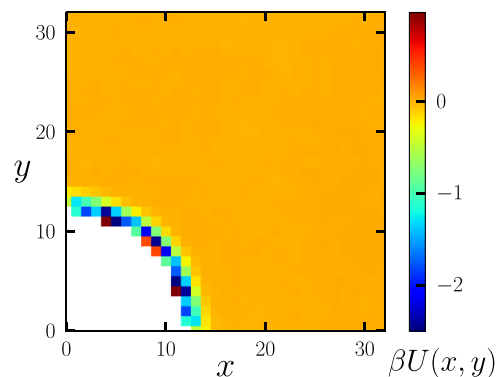
contact between the disks, $s=0$, is about 5 times deeper than for $\Delta\mu_s=0$. Moving further into the *A*-rich phase, $\Delta\mu_s=-0.2$, the strength of the attraction is reduced. More strikingly, the range is dramatically reduced and the potential becomes “sticky.” This variation of $U(s)$ with $\Delta\mu_s$ leads to a characteristic variation in the reduced second virial coefficient, B_2^* — see Fig. 4 in Ref. 1. The net attraction between the colloids is strongest at off-critical compositions of the solvent, consistent with results of studies of the critical Casimir attraction between walls.^{11,27,28}

As we model the colloid-fluid interactions via nearest neighbour interactions, and the surface perimeter of our colloid is discretized, the effective two-body potential between colloids is not smooth. Therefore certain solvent sites right next to the colloid can have more than one colloid site as its neighbour, as is clear from Fig. 2. The surface field induced by the colloid is not homogeneous and under certain conditions this heterogeneity plays an important role.

In Figure 14 we plot the effective two-body potential between colloids of radius $R=6$ with $\alpha=0.6$, determined at $\Delta\mu_s=-0.01$ and $\Delta\mu_s=-0.5$, for temperature $\tau=0.05$. The effective potential close to the surface of the colloid is heterogeneous for both chemical potentials, i.e., $U(x,y) \neq U(x^2+y^2)$. It turns out that these lattice effects can have a pronounced effect on phase coexistence. The lattice effects



(a)



(b)

FIG. 14. Effective two-body potential, $U(x,y)$, between two colloids of radius $R=6$ and $\alpha=0.6$ suspended in a solvent at $\tau=0.025$ for (a) $\Delta\mu_s=-0.01$ and (b) $\Delta\mu_s=-0.5$. The area in white is inaccessible due to the hard-core repulsion. For $(x^2+y^2)^{1/2} \approx 2R$, the potential displays lattice-induced heterogeneity.

play no role in G-L coexistence where typically a solvent film spanning several lattice sites is found preferentially adsorbed on the surface of a colloid and the range of the effective interaction is many lattice sites, as in Fig. 14(a). However, they do play a significant role in G-X coexistence, i.e., the crystal phase is facilitated by the colloids aligning along the more energetically favourable directions. Recall that the crystal phase typically becomes stable for $\Delta\mu_s \lesssim -0.1$ (see Fig. 7) where for $\alpha = 0.6$, m_B , the fraction of BC surface interactions is $\lesssim 0.5$ (see Fig. 10). In this regime it is the relatively low surface occupancy that determines the short-range of the effective potential: this is only 1-3 lattice sites in Fig. 14(b).

In our earlier study¹ we reported results of simulations of the colloidal phase diagram for an effective system, namely one in which the colloidal particles interact solely via the pair potential $U(r)$ determined at solvent state points ($\Delta\mu_s$ and τ) as described above. We re-iterate that whilst the effective system does exhibit G-L and G-X coexistence, the G-L binodals are not close to those computed for the full ternary mixture with $R = 6$ and $\alpha = 0.6$ —see Fig. 4(d) of Ref. 1. In particular the pair-potential treatment overestimates the extent of G-L coexistence and underestimates the shift of the critical point from that of the solvent reservoir. We return to this point later. Once more, we note that lattice effects are not important for G-L coexistence. On the other hand, the effective pair-potential treatment provides a rather good account of G-X coexistence, i.e., the binodals for $\Delta\mu_s < -0.1$ in Figure 7, provided lattice effects are incorporated properly. From our present study we conclude that an effective-pair potential treatment can capture the gross features of the phase behaviour but is very unlikely to provide a quantitative description. It would be instructive to perform detailed comparisons for other radii and wettability strength.

V. CONCLUSION

Using a simple lattice model we have investigated the phase behaviour of colloidal particles immersed in near-critical solvents. Our model is a minimal one for treating colloidal self-assembly mediated by the long-ranged effective interactions that arise from long-ranged correlations in an explicit solvent. The choice of model was motivated in Sec. II. The size asymmetry between the (big) colloid and the (small) solvent particles and the requirement to treat a dense solvent grand canonically set severe computational demands. In addition, having accurate estimates of the binodal of the colloid-free solvent and knowledge of the solvent's adsorption (wetting) properties at the surface of a single (very large) colloid are important prerequisites. Such considerations led us to treat a 2D lattice model for the AB solvent, incorporating hard disks representing the colloids (C), that was introduced in a recent Letter.¹ There we presented results for the phase behaviour of the ABC model for colloids of a particular radius $R = 6$ and colloid-solvent adsorption strength (wettability) $\alpha = 0.6$. In the present work we have provided details of the computer simulation methods employed and extended our earlier study by (i) investigating systematically the phase

behaviour of our model as a function of R and α , and (ii) by determining the structure of the ternary liquid mixture.

In Ref. 1 we found that the critical point of the ternary colloid-solvent mixture shifts significantly from that of the colloid-free solvent upon adding a small volume fraction η of colloids. Here we show that on increasing α , i.e., the preference of colloid C for species B , at a fixed reduced temperature τ and radius $R = 6$, the G-L binodals broaden and the G-L critical point shifts towards the critical point of the solvent. However, there is a saturation value of α above which the phase coexistence is unchanged. For the data shown in Fig. 11, the saturation value of α is ≈ 5.0 . The phase behaviour with respect to the size of the colloid R is arguably more important than that with respect to α . Upon increasing R at fixed τ and α , the G-L binodal becomes much flatter, and the critical point shifts to larger colloid fraction η (see Figure 12). Unfortunately, investigating larger values of R pertinent to the regime of real colloidal systems is constrained by computational resources. It is significant that the trends found by increasing both α and R are similar to those found in the mean-field treatment of Ref. 37 for the same model. This observation suggests that excluded volume considerations, incorporated in the mean-field treatment, are important in determining G-L coexistence and, indeed, the overall phase behaviour of our model.

One of the key advantages of our ternary mixture model is that it enables us to investigate fractionation of the solvent; the composition x of the solvent is generally different from that of the solvent reservoir x_r . This is illustrated (see Fig. 8) for coexisting colloidal liquid and gas phases. In the dense liquid phase, L , the solvent is very rich in the solvent species B favoured by the colloids. In principle we could calculate the values of x from our simulation results for the two coexisting phases. That would allow us to make further contact with the mean-field treatment of Ref. 37. Note that unlike the results for $\Delta\mu_s$ versus η shown here and those for x_r versus η given in Fig. 3(c) of Ref. 1, the tie-lines are not horizontal in the x versus η representation—see Fig. 3 of Ref. 37. Fractionation arises naturally in our approach that treats a full ternary mixture. By contrast, approaches such as those of Mohry *et al.*¹¹⁻¹³ and Nguyen *et al.*³⁶ that treat the solvent as an implicit background, whose role is merely to induce an effective pairwise colloid-colloid interaction, struggle to incorporate this important element of the physics of the phase behaviour.

Results for the partial structure factors shed further light on the nature of criticality in our model ternary mixture. Sufficiently close to a critical point, all the partial structure factors $S_{ab}(k)$ exhibit Ornstein-Zernike-like (OZ) behaviour at small wavenumbers k characterized by a single (OZ) correlation length. We chose to focus on $S_{BB}(k)$, i.e., on solvent species BB correlations. However, we could equally have measured the BC or CC partial structure factors. Although these are quite different from $S_{BB}(k)$ plotted in Fig. 9(a), the modulus of each $S_{ab}(0)$ should exhibit the same dependence on η as that shown in Fig. 9(b). That is, proximity to the critical point is signalled by a diverging $S_{ab}(0)$ for any ab pair. This phenomenon of “critical point infection” is manifest more directly in real space. The quantity $r^{(D-1)/2}(g_{ab}(r) - 1)$,

as $r \rightarrow \infty$, decays exponentially with a common correlation length ξ .⁶² Here, $g_{ab}(r)$ is the pair correlation function for species ab and, as before, D is the spatial dimension. As the critical point is approached, ξ diverges.

Now consider an extremely dilute colloidal suspension that may or may not be close to criticality of the solvent, where the colloid volume fraction $\eta \rightarrow 0$. Then, for mixtures where all species interact with short-ranged potentials, $r^{(D-1)/2}(g_{CC}(r) - 1)$ decays as $e^{-r/\xi}$ where, in the dilute colloid limit, ξ is determined by correlations in the pure solvent. In this limit, $g_{CC}(r) = \exp(-\beta\phi_{\text{eff}}(r))$, and it follows that the effective colloid-colloid pair potential $\phi_{\text{eff}}(r)$ must decay as $e^{-r/\xi}/r^{(D-1)/2}$ as $r \rightarrow \infty$. Suppose now the solvent is only very slightly removed from its criticality. The solvent correlation length ξ is long and sets the length scale determining the range of $\phi_{\text{eff}}(r)$. This simple argument describes the origin of the tail of the critical Casimir interaction between two identical colloids in the framework of liquid mixtures. Suppose now we have a more concentrated suspension of colloids. Measuring $S_{CC}(k)$ or $g_{CC}(r)$ at given η , τ and x_r will yield the correlation length of the concentrated ternary mixture, not that of the pure solvent, under the given conditions. This observation is relevant for experimental work^{34,35} that attempts to extract a reliable $\phi_{\text{eff}}(r)$, characteristic of the pure solvent, from measurements of $g_{CC}(r)$. Performing an experiment that extracts reliable data in the dilute limit is not straightforward. Given that the critical point shifts rapidly with η , values extracted for ξ , and hence $\phi_{\text{eff}}(r)$, are likely to be very sensitive to η .

We have focused on the supercritical regime of the solvent phase diagram—the box in Fig. 1. The same ABC model and computational techniques could be used to investigate the subcritical region of the solvent reservoir. In this regime ($\tau < 0$, $\Delta\mu_s < 0$) strong preferential adsorption can lead to a bridging transition⁶⁵ between two identical colloidal particles. This is equivalent to rounding the well-known capillary condensation transition of a binary mixture confined between two identical planar substrates.⁵⁶ Once again it is important that the bulk solvent prefers species A , while the colloids prefer the phase rich in B , leading to a capillary bridge of the latter phase. The resulting SM interaction can be strongly attractive.^{66–70} Unlike the critical Casimir SM interactions, these non-critical interactions are non-universal and are dependent on the precise nature of the local interactions between a colloid and the binary solvent at the given state point. Our model can incorporate these. Indeed we have observed bridging phenomena in our simulations under subcritical conditions.

The results presented here are relevant to experimentally realisable quasi-2D systems such as protein assembly in plasma membranes of living cells where it is argued Critical Casimir forces might arise between macromolecules embedded in a biomembrane,^{71,72} an observation that has spurred careful density matrix renormalization group calculations of the scaled Casimir force between disks.⁷³ In our earlier discussion we implied that our results should also be relevant to 3D systems. The results of a mean-field theory presented in Ref. 37 suggest that the fine details of solvent criticality, specifically the precise nature of two-body critical Casimir forces, are not too important in determining the main

features of the observed phase coexistence. Thus, we speculate that the phase behaviour in 3D will be qualitatively similar to the currently investigated 2D case. Preliminary results from simulations of a 3D system of hard spheres embedded in a 3D AB lattice-gas, which we hope to publish in the near future, appear to confirm our speculation.

Equipped with this insight, we conclude by returning to two pertinent experimental studies of near-critical colloidal aggregation. We focus first on the pioneering study of Beysens and Estève,¹⁷ mentioned in Section I, who used light scattering to investigate silica colloids suspended in a water-lutidine mixture. Recall this solvent exhibits a lower demixing critical point with $T_c = 34^\circ$ and lutidine mass fraction of $x_c = 0.286$. The colloids prefer lutidine over water and in Fig. 2 of Ref. 17, the authors plot the thickness of the lutidine layer adsorbed on a silica colloid. At fixed solvent concentrations x_{Lu} lying slightly below x_c , the thickness increases rapidly with increasing temperature until the aggregation line is reached; this lies about 0.4 K below the binodal. The observed increase in layer thickness at state points approaching the aggregation line, residing in the water-rich region, is a signature that strong preferential adsorption drives the aggregation phenomenon. The inset to our Fig. 5 shows that the (excess) adsorption, obtained by integrating the density profiles, increases rapidly with decreasing τ , approaching the critical point. Fig. 4(a) of Ref. 1 shows the thickness of the B -rich film increasing with decreasing τ , for $\Delta\mu_s$ slightly negative, corresponding to solvent compositions slightly below $x_{r,c}$. Clearly our model system incorporates correctly the preferential adsorption at a single colloid. It also incorporates the crucial competition between the bulk solvent preferring a certain species (A) and the colloid preferring another (B), which drives the aggregation. In a typical experiment a fixed number of colloids is suspended in a solvent at fixed composition, x_r , and the temperature is changed to induce (reversibly) aggregation. Then, for fixed η , the locus of points in the T versus x_r plane, where aggregation is first observed, is termed an aggregation line—see, e.g., Fig. 3 in Ref. 17. In Ref. 37 aggregation lines were calculated using the mean-field treatment, taking the view that aggregation corresponds to the onset of colloidal phase separation. Results are shown for $\eta = 0.05$ and 0.1 in Fig. 5 of this paper. The shape of the aggregation lines is similar to that shown in Ref. 17 when we recognize that our model has an upper, rather than a lower, demixing critical point. In principle we could also compute aggregation lines from our simulation results but this would be hugely expensive. Given the mean-field treatment captures the main features of the simulation phase diagrams, we would expect to find the same shapes for aggregation lines from our simulations. Quantitative comparisons with experiment are inappropriate. In Ref. 17 results near aggregation imply the ratio ξ/R is at most 0.2 which should be contrasted with a typical value of about 3 from theory and simulation.³⁷

The second experimental study we consider is the confocal microscopy (real-space) investigation³⁴ of poly-*n*-isopropyl acrylamide (PNIPAM) colloidal particles suspended in quasi-binary solvent of 3-methyl pyridine, water, and heavy water which has a lower critical temperature and a critical methyl pyridine mass fraction $x_c = 0.31$. PNIPAM particles

swell in the solvent; near the critical point the particle radius was about 250 nm. In the experiments the initial packing fraction was about 0.02 and the mass fraction of methyl pyridine was fixed at 0.25, i.e., substantially below the critical composition. Remarkably, upon increasing the temperature towards that of the solvent binodal, colloidal gas, liquid, and crystal phases were observed. Specifically, condensed, liquid-like aggregates were first observed at 0.3 K below the temperature of the solvent binodal, and upon raising the temperature a further 0.1 K the particles inside the aggregates formed an ordered fcc crystal.³⁴ Although our model certainly yields stable gas, liquid and crystal phases it is not clear that it can account for the sequence of phases found in Ref. 34. As observed in Ref. 37, changing the composition of the solvent reservoir does lead to considerable variation in the τ versus η phase diagrams of our model. Making direct comparisons is not straightforward. Given the PNIPAM particles are very large and there is substantial deviation from the critical composition, the ratio ξ/R is very small in these experiments and is typically much smaller than in the regime investigated in the present study. Therefore one should not rule out the possibility that aggregates observed in Ref. 34 arise from specific (non-universal) solvent-mediated interactions. Whether these are captured properly by the “Casimir” pair potentials extracted from measurements of $g_{CC}(r)$ in the dilute colloidal gas is open to discussion. Bearing in mind the ratios of length scales, our study is, perhaps, more representative of nanoparticles suspended in a near-critical solvent. In this respect it suggests that such systems might exhibit very rich phase diagrams with the potential for a wide range of colloidal self-assembly controlled by sensitive tuning of temperature and solvent composition.

ACKNOWLEDGMENTS

We thank N. Wilding, D. Ashton, and A. Maciolek for stimulating discussions. N.T. and M.D. acknowledge financial support from an NWO-ECHO grant. J.R.E. and M.D. acknowledge financial support from a Nederlandse Organisatie voor Wetenschappelijk Onderzoek (NWO) VICI grant. N.T., J.R.E., M.D. acknowledge a NWO-EW grant for computing time on the Dutch supercomputer Cartesius. R. Evans is grateful for the hospitality of the members of the Debye Institute, Utrecht on his frequent visits and to the Leverhulme Trust for the award of an Emeritus Fellowship No. EM-2016-031. This work is part of the D-ITP consortium, a program of the Netherlands Organisation for Scientific Research (NWO) funded by the Dutch Ministry of Education, Culture and Science (OCW).

¹J. R. Edison, N. Tasios, S. Belli, R. Evans, R. van Roij, and M. Dijkstra, *Phys. Rev. Lett.* **114**, 038301 (2015).

²G. Flöter and S. Dietrich, *Z. Phys. B: Condens. Matter* **97**, 213 (1995).

³M. Fisher and P. Gennes, *C. R. Acad. Sci. B Phys.* **287**, 207 (1978).

⁴M. Krech and S. Dietrich, *Phys. Rev. Lett.* **66**, 345 (1991).

⁵M. Krech and S. Dietrich, *Phys. Rev. A* **46**, 1922 (1992).

⁶M. Krech, *The Casimir Effect in Critical Systems* (World Scientific, 1994).

⁷H. B. G. Casimir, *Kon. Ned. Akad. Wetensch. Proc.* **51**, 793 (1948).

⁸A. Hanke, F. Schlesener, E. Eisenriegler, and S. Dietrich, *Phys. Rev. Lett.* **81**, 1885 (1998).

⁹O. Vasilyev, A. Gambassi, A. Maciolek, and S. Dietrich, *Phys. Rev. E* **79**, 041142 (2009).

¹⁰B. Derjaguin, *Kolloid-Z.* **69**, 155 (1934).

¹¹T. F. Mohry, S. Kondrat, A. Maciolek, and S. Dietrich, *Soft Matter* **10**, 5510 (2014).

¹²T. Mohry, A. Maciolek, and S. Dietrich, *J. Chem. Phys.* **136**, 224902 (2012).

¹³T. Mohry, A. Maciolek, and S. Dietrich, *J. Chem. Phys.* **136**, 224903 (2012).

¹⁴C. Hertlein, L. Helden, A. Gambassi, S. Dietrich, and C. Bechinger, *Nature* **451**, 172 (2008).

¹⁵A. Gambassi, A. Maciolek, C. Hertlein, U. Nellen, L. Helden, C. Bechinger, and S. Dietrich, *Phys. Rev. E* **80**, 061143 (2009).

¹⁶A. Maciolek and S. Dietrich, “A review by A. Maciolek and S. Dietrich” (unpublished).

¹⁷D. Beysens and D. Estève, *Phys. Rev. Lett.* **54**, 2123 (1985).

¹⁸P. Gallagher, M. Kurnaz, and J. Maher, *Phys. Rev. A* **46**, 7750 (1992).

¹⁹P. Gallagher and J. Maher, *Phys. Rev. A* **46**, 2012 (1992).

²⁰T. Narayanan, A. Kumar, E. Gopal, D. Beysens, P. Guenoun, and G. Zalczer, *Phys. Rev. E* **48**, 1989 (1993).

²¹S. R. Kline and E. W. Kaler, *Langmuir* **10**, 412 (1994).

²²Y. Jayalakshmi and E. W. Kaler, *Phys. Rev. Lett.* **78**, 1379 (1997).

²³B. Rathke, H. Grull, and D. Woermann, *J. Colloid Interface Sci.* **192**, 334 (1997).

²⁴R. D. Koehler and E. W. Kaler, *Langmuir* **13**, 2463 (1997).

²⁵J. S. van Duijneveldt and D. Beysens, *J. Chem. Phys.* **94**, 5222 (1991).

²⁶D. Beysens and T. Narayanan, *J. Stat. Phys.* **95**, 997 (1999).

²⁷A. Drzewiński, A. Maciolek, and R. Evans, *Phys. Rev. Lett.* **85**, 3079 (2000).

²⁸R. Okamoto and A. Onuki, *J. Chem. Phys.* **136**, 114704 (2012).

²⁹T. Sluckin, *Phys. Rev. A* **41**, 960 (1990).

³⁰H. Löwen, *Phys. Rev. Lett.* **74**, 1028 (1995).

³¹R. R. Netz, *Phys. Rev. Lett.* **76**, 3646 (1996).

³²T. Gil, J. H. Ipsen, and C. F. Tejero, *Phys. Rev. E* **57**, 3123 (1998).

³³H. Guo, T. Narayanan, M. Sztuchi, P. Schall, and G. H. Wegdam, *Phys. Rev. Lett.* **100**, 188303 (2008).

³⁴V. D. Nguyen, S. Faber, Z. Hu, G. H. Wegdam, and P. Schall, *Nat. Commun.* **4**, 1584 (2013).

³⁵M. T. Dang, A. V. Verde, P. G. Bolhuis, P. Schall *et al.*, *J. Chem. Phys.* **139**, 094903 (2013).

³⁶V. Nguyen, M. Dang, T. Nguyen, and P. Schall, *J. Phys.: Condens. Matter* **28**, 043001 (2016).

³⁷J. R. Edison, S. Belli, R. Evans, R. van Roij, and M. Dijkstra, *Mol. Phys.* **113**, 2546 (2015).

³⁸K. Binder, A. M. Ferrenberg, and D. P. Landau, *Ber. Bunsen-Ges.* **98**, 340 (1994).

³⁹D. Nicolaidis and R. Evans, *Phys. Rev. B* **39**, 9336 (1989).

⁴⁰R. Evans and U. M. B. Marconi, *J. Chem. Phys.* **86**, 7138 (1987).

⁴¹M. E. J. Newman and G. T. Barkema, *Monte Carlo Methods in Statistical Physics* (Clarendon Press; Oxford University Press, New York, 1999).

⁴²J. R. Heringa and H. W. J. Blöte, *Phys. Rev. E* **57**, 4976 (1998).

⁴³H. Hobrecht and A. Hucht, *Phys. Rev. E* **92**, 042315 (2015).

⁴⁴E. Rabani, D. R. Reichman, P. L. Geissler, and L. E. Brus, *Nature* **426**, 271 (2003).

⁴⁵A. Z. Panagiotopoulos, *J. Chem. Phys.* **112**, 7132 (2000).

⁴⁶A. Z. Panagiotopoulos, *J. Chem. Phys.* **123**, 104504 (2005).

⁴⁷K. E. Gubbins, *Mol. Simul.* **2**, 223 (1989).

⁴⁸D. J. Ashton and N. B. Wilding, *Mol. Phys.* **109**, 999 (2011).

⁴⁹F. A. Escobedo and F. J. Martínez-Veracochea, *J. Chem. Phys.* **127**, 174103 (2007).

⁵⁰F. A. Escobedo, *J. Chem. Phys.* **127**, 174104 (2007).

⁵¹A. Z. Panagiotopoulos, *J. Phys.: Condens. Matter* **12**, R25 (2000).

⁵²G. Latouche, *Level-Independent Quasi-Birth-and-Death Processes* (John Wiley & Sons, Inc., 2010).

⁵³G. Bolch, S. Greiner, H. de Meer, and K. Trivedi, *Queueing Networks and Markov Chains: Modeling and Performance Evaluation with Computer Science Applications* (Wiley, 2006).

⁵⁴L. Onsager, *Phys. Rev.* **65**, 117 (1944).

⁵⁵R. Pandit, M. Schick, and M. Wortis, *Phys. Rev. B* **26**, 5112 (1982).

⁵⁶R. Evans, *J. Phys.: Condens. Matter* **2**, 8989 (1990).

⁵⁷P. Pieranski, *Phys. Rev. Lett.* **45**, 569 (1980).

⁵⁸K. A. Maerzke, L. Gai, P. T. Cummings, and C. McCabe, *J. Phys.: Conf. Ser.* **487**, 012002 (2014).

⁵⁹F. Del Rio, E. Avalos, R. Espindola, L. F. Rull, G. Jackson, and S. Lago, *Mol. Phys.* **100**, 2531 (2002).

⁶⁰L. Vega, E. de Miguel, L. F. Rull, G. Jackson, and I. A. McLure, *J. Chem. Phys.* **96**, 2296 (1992).

- ⁶¹D. L. Pagan and J. D. Gunton, *J. Chem. Phys.* **122**, 184515 (2005).
- ⁶²R. Evans, R. J. F. Leote de Carvalho, J. R. Henderson, and D. C. Hoyle, *J. Chem. Phys.* **100**, 591 (1994).
- ⁶³J. Hansen and I. McDonald, *Theory of Simple Liquids*, 3rd ed. (Academic Press, 2006).
- ⁶⁴O. A. Vasilyev, *Phys. Rev. E* **90**, 012138 (2014).
- ⁶⁵H. T. Dobbs, G. A. Darbellay, and J. M. Yeomans, *Europhys. Lett.* **18**, 439 (1992).
- ⁶⁶C. Bauer, T. Bieker, and S. Dietrich, *Phys. Rev. E* **62**, 5324 (2000).
- ⁶⁷P. Hopkins, A. J. Archer, and R. Evans, *J. Chem. Phys.* **131**, 124704 (2009).
- ⁶⁸R. Okamoto and A. Onuki, *Phys. Rev. E* **88**, 022309 (2013).
- ⁶⁹P. J. Upton, J. O. Indekeu, and J. M. Yeomans, *Phys. Rev. B* **40**, 666 (1989).
- ⁷⁰A. J. Archer, R. Evans, R. Roth, and M. Oettel, *J. Chem. Phys.* **122**, 084513 (2005).
- ⁷¹S. L. Veatch, P. Cicuta, P. Sengupta, A. Honerkamp-Smith, D. Holowka, and B. Baird, *ACS Chem. Biol.* **3**, 287 (2008).
- ⁷²B. B. Machta, S. L. Veatch, and J. P. Sethna, *Phys. Rev. Lett.* **109**, 138101 (2012).
- ⁷³M. Zubaszewska, A. Maciołek, and A. Drzewiński, *Phys. Rev. E* **88**, 052129 (2013).